Impact of spatially-variable soil thickness and texture on simulated hydrologic conditions in a semiarid watershed in northwest Mexico

Luis A. Méndez-Barroso[1, 2*], Enrique R. Vivoni[2,3], and Giuseppe Mascaro[3, 4]

[1] *Departamento de Ciencias del Agua y del Medio Ambiente, Instituto Tecnológico de Sonora, Ciudad Obregón, Sonora, C.P. 85000, Mexico.*
[2] *School of Earth and Space Exploration, Arizona State University, Tempe, Arizona, United States of America.*
[3] *School of Sustainable Engineering and the Built Environment, Arizona State University, Tempe, Arizona, United States of America.*
[4] *Julie Ann Wrigley Global Institute of Sustainability, Arizona State University, Tempe, Arizona, United States of America.*
**lmendezb@asu.edu, luis.mendez@itson.edu.mx*

ABSTRACT

Soil depth and texture exert strong controls on the spatial distribution of water and energy fluxes and states in semiarid watersheds. As a result, realistic representations of the spatial soil characteristics within watersheds are important for the improvement of process-based distributed hydrologic modeling applications. In this study, we evaluated the effects of combinations of soil thickness and soil texture products with varying spatial distributions to assess their effects on the simulated hydrologic response in the semiarid Sierra Los Locos watershed in Sonora, Mexico. The main findings of the hydrological simulations show that soil texture exerted a strong control on evapotranspiration and soil moisture patterns, while soil thickness was directly related with the magnitude and range of the simulated values. Furthermore, soil texture patterns were an important factor controlling the spatial and temporal persistence of soil moisture which is highly evident during the transition from dry to wet conditions in the North American monsoon region**.** Once vegetation cover increases in the watershed in response to seasonal rainfall, the influence of soil texture decreases for determining the spatial distribution of the simulated hydrologic response and soil thickness becomes more important. Spatially-variable soil thickness tends to create soil depressions that store and transmit subsurface water, leading to large spatial variations in soil moisture, evapotranspiration and runoff generation. The results of this study highlight the sensitivity of estimated water fluxes and states with respect to the spatial distribution of soil depth and texture as obtained in a distributed hydrologic model representative of modern approaches. Finally, this research work offers insight into the importance of field studies and remote sensing approaches to better characterize these watershed properties.

Key words: Distributed hydrologic modeling; soil depth; sensitivity analysis; arid and semiarid hydrology; spatial patterns, Sierra Los Locos; Sonora; Mexico.

RESUMEN

La profundidad y textura del suelo ejercen un control fuerte sobre la distribución espacial de los flujos de agua y energía en cuencas semiáridas. Como resultado, la representación espacial realística de las características del suelo son de suma importancia para el mejoramiento de las aplicaciones de los modelos hidrológicos basados en procesos. En este estudio evaluamos los efectos de diferentes combinaciones de varias distribuciones espaciales del espesor de suelo y su textura para estimar sus efectos en la respuesta de simulaciones hidrológicas en la cuenca semiárida Sierra Los Locos en Sonora, México. Los principales resultados de las simulaciones hidrológicas muestran que la textura de suelo ejerce un fuerte control en los patrones espaciales de evapotranspiración y humedad de suelo mientras que el grosor del suelo está directamente relacionado con la magnitud y rango de los valores simulados. Además, los patrones de distribución de textura de suelo fueron un factor muy importante en el control de la persistencia temporal y espacial de humedad de suelo la cual es muy evidente durante la transición de condiciones secas a húmedas en la región del Monzón de Norteamérica.

Méndez-Barroso, L.A., Vivoni, E.R., Mascaro, G., 2016, Impact of spatially-variable soil thickness and texture on simulated hydrologic conditions in a semiarid watershed in northwest Mexico: Revista Mexicana de Ciencias Geológicas, v. 33, núm. 3, p. 365-377.

Una vez que la cobertura vegetal se incrementa en la cuenca en respuesta a la estacionalidad de la lluvia, la influencia de la textura de suelo decrece en la determinación de la distribución espacial de la respuesta hidrológica simulada y la profundidad del suelo comienza a ser más importante. El espesor del suelo variable en el espacio tiende a crear depresiones por debajo de la superficie que almacena y trasmite agua subterránea, dando lugar a grandes variaciones en humedad del suelo, evapotranspiración y generación de escorrentía. Los resultados de este estudio ponen de manifiesto la sensibilidad de los estados y flujos de agua estimados con respecto a la distribución espacial de la profundidad y textura del suelo obtenido en un modelo hidrológico distribuido representativo de enfoques modernos. Finalmente, este trabajo de investigación ofrece una idea de la importancia de los estudios de campo y métodos de teledetección para caracterizar mejor las propiedades de las cuencas hidrográficas

Palabras clave: Modelo hidrológico distribuido; profundidad del suelo; análisis de sensibilidad; hidrología; zonas áridas; zonas semiáridas; patrones espaciales; Sierra Los Locos; Sonora; México.

INTRODUCTION

Soil depth and texture exert strong controls on water and energy fluxes at the ground surface affecting their spatiotemporal distributions in watersheds (Saxton and Rawls, 2005; English *et al.*, 2005). It is widely accepted that thin soils lead to the production of saturation-excess overland runoff, while thicker soils have more storage capacity, thus controlling biotic and abiotic processes (Bertoldi *et al.*, 2006; Tromp-Van Meerveld and McDonnell, 2006; Gochis *et al.*, 2010). Soil depth (or thickness) acts as a main reservoir for water in semiarid watersheds and affects plant transpiration and carbon fixation in ecosystems depending on the temporal and spatial availability of soil moisture. Similarly, soil texture (or particle size distribution) controls the storage and infiltration capacity of a soil profile leading to variations in soil water content and its dependent hydrologic processes. For these reasons, accurate spatial representations of soil depth and texture are important to identify the spatial patterns of hydrologic processes and their connectivity, as well as their persistence in time and space (*e.g.*, Vivoni *et al.*, 2008a; Pelletier and Rasmussen, 2009; Nicótina *et al.*, 2011). Nevertheless, these soil properties are highly variable within a watershed due to the complex interactions between topography, climate and biophysical processes. Thus, determining the spatial distribution of soil thickness and texture remains an open question in Geosciences.

The use of topographic attributes, such as elevation, slope and curvature, is a promising approach for estimating the spatial distribution of soil depth. A common set of methods is based on empirical relations between local terrain attributes and the soil thickness observed at a limited number of sampling sites (*e.g.*, Moore *et al.*, 1993; Gessler *et al.*, 1995; Saulnier *et al.*, 1997; Heimsath *et al.*, 1999, Catani *et al.*, 2010). These methods have the capacity to overcome the need for a large number of soil depth observations that are difficult and time-consuming to obtain. When soil thickness varies spatially within a watershed, we would expect significant spatial differences in soil moisture, evapotranspiration and runoff production dictated by the soil depth patterns. Identifying whether this is the case is possible through the use of a numerical watershed model that accounts for the hydrologic processes in semiarid regions where terrain attributes have a strong control on soil distributions. Only a few studies have focused on the importance that soil thickness exerts on hydrologic processes in semiarid regions with complex topography (*e.g.*, Gochis *et al.*, 2010; Cuo *et al.*, 2011 ; Rahimy, 2012; Garambois *et al.*, 2013). However, in these studies, the spatial patterns of hydrologic states and fluxes typically have not been investigated. Furthermore, the controls of soil texture and its interaction with soil depth are often ignored by, for example, assuming a homogeneous soil type in the watershed.

Including the spatial distribution of soil texture is essential for depicting hydrologic properties, such as hydraulic conductivity, porosity and water holding capacity. Nevertheless, existing soil texture maps are often very coarse since these are based on limited soil sampling sites and interpolations using mapped topographic or geological units. Recent studies have shown that soil texture correlates with radiances in the visible and near infrared regions (Zhang *et al.*, 1992; Sullivan *et al.*, 2005). This characteristic allows for the use of multi-band remote sensing imagery to infer soil texture from satellites at high spatial resolutions (ranging from 15 to 90 m, depending on the satellite used). The role played by the spatial distribution of soil texture on the hydrologic response in a watershed can be quantified using a numerical watershed model able to represent the spatial variations in soil hydrologic properties at high resolution. This spatial control is often ignored in modeling studies which assume a single soil texture map that is typically coarser in resolution than the terrain or vegetation properties represented in the model.

In this study, we evaluate the effects of distributed soil depth and texture representations on the water and energy fluxes within a semiarid watershed of northwest Mexico. The study site was selected for its complex terrain leading to spatial variations in both soil depth and texture that affect hydrologic conditions during a wet summer season related to the North American monsoon (NAM). Thus, while the region is considered to be semiarid, Vivoni *et al.* (2010) suggest that the watersheds in the NAM region are 'seasonally wet' with sufficient soil moisture to induce downslope lateral transport that is impacted by the distribution of soil depth. The arrival of intense storms during the NAM (Mascaro *et al.*, 2014) also implies that the soil textural controls on infiltration-excess overland flow are important within the watershed. We combine a diverse set of tools and datasets in this study, including: (1) a distributed hydrologic model tested thoroughly against field observations (Vivoni *et al.*, 2010; Méndez-Barroso *et al.*, 2014), (2) a set of soil depth observations including particle size distribution and (3) geospatial data layers from remote sensing used to conduct terrain analyses and soil mapping. Simulations during the Soil Moisture Experiment 2004 (SMEX04) were conducted for different combinations of soil depth and texture maps with a hydrologic model known as the Triangulated Irregular Network (TIN)-based Real-time Integrated Basin Simulator (tRIBS, Ivanov *et al.*, 2004; Vivoni *et al.*, 2007b). This hydrologic model has been used effectively in prior studies to identify the controls related to terrain and soil conditions on the spatial patterns of the hydrologic response (*e.g.*, Vivoni *et al.*, 2010; Mahmood and Vivoni, 2011; Robles-Morúa *et al.*, 2012), but the combined sensitivity to spatial representations of soil depth and texture has not been investigated.

Although we have tested only one model, the hydrological model tRIBS shares common features with a wide range of process-based (or physically-based) hydrological models. Many current process-based models basically share the same structure in terms of process description, techniques of solution and model approach (see reviews by Singh *et al.*, 2002; Fatichi *et al.*, 2016). Modern process-based hydrological models (such as tRIBS) represent or estimate water fluxes and states by incorporating the spatial variability of meteorological forcings, the representation of the topographic features and the heterogeneity of land surface characteristics. At the same time, these models can resolve the lateral and vertical subsurface fluxes within a representative elemental unit. Therefore, these models require solving partial differential equations in three spatial dimensions and time which require numerical methods such as finite difference or finite element techniques. Similarly,

tRIBS and other hydrological models are based on the integration of multiple process components that represents the dynamics in a watershed at a higher integrated scale. This latter is known as "bottom up" model approach. Furthermore, flow pathways in distributed process-based models, especially for shallow groundwater movement, typically rely on the assumption that these pathways are controlled by catchment topography. However, this assumption is valid for shallow soils underlain by impermeable bedrock. Recent modeling research has found that bedrock topography exerts a stronger control in downslope groundwater flows rather than surface topography (MacDonell *et al*., 1996). Despite these recent findings, the role of bedrock topography on the spatial variations of groundwater fluxes and the generation of runoff is still poorly understood.

METHODS

Study Watershed

The study watershed is the Sierra Los Locos (SLL, 93.2 km^2) basin located east of the small rural town of Opodepe, Sonora, and about 150 km northeast of Hermosillo, Sonora, Mexico. Figure 1 shows the location of SLL watershed that is nested inside the Rio San Miguel (3,796 km^2) with its elevation characteristics. Elevation data at 30 m resolution from the Advance Spaceborne Thermal Emission and Reflection Radiometer (ASTER) was utilized to derive the topographic attributes (*e.g.*, elevation, slope, curvature and topographic index) as well as the watershed boundary and stream network. Total relief in the watershed is 1,035 m, with the lower elevations dominated by subtropical scrubland, while oak woodlands and grasses dominate higher elevations (Vivoni *et al*., 2007a, 2010; Méndez-Barroso *et al*., 2009; Méndez-Barroso and Vivoni, 2010). Local topography influences the mean annual rainfall, which ranges from 500 to 700 mm/yr, with close to 70% of the annual amounts falling during the NAM from July to September (Xiang *et al*., 2014; Mascaro *et al*., 2014). Several studies in the NAM region have shown that rainfall seasonality leads to large changes in vegetation greenness which affect water and energy fluxes (*e.g.*, Dominguez *et al*., 2008; Forzieri *et al*., 2011, 2014; Tang *et al*., 2012; Vivoni, 2012; Méndez-Barroso *et al*., 2014). As a result, it is important to incorporate the seasonal variations in rainfall and vegetation properties when identifying the role of soil thickness and texture on the spatial distribution of hydrologic processes in the watershed during the North American monsoon. As described later, the hydrologic model used here has the capability to account for dynamic changes of vegetation properties and hydrometeorological forcings.

Soil thickness and soil texture sampling

Two soil sampling activities were carried out in August 2007 in the SLL watershed (Vivoni *et al*., 2010), consisting of: (1) the estimation of soil depth from six soil pits and (2) the sampling of surface soils (0 to 5 cm depth) at forty-two locations distributed from the basin headwaters to the outlet. Because of limitations in site accessibility, we focused the sampling activities close to the main unpaved road traversing the watershed along an elevation transect. Figure 1b shows the location of soil pits (dark squares) and surface soil samples (triangles). Soil pit records, containing soil thickness and texture, were obtained at representative locations with varying characteristics such as elevation, slope and vegetation cover. The soil thickness was determined when an impermeable soil horizon was found. Soil samples were analyzed in the laboratory to determine particle size distribution (texture) and bulk density. Bulk density was estimated by the clod method (Blake, 1965), while the relative masses of sand, silt and clay were obtained through the "Pipette" method (Gee and Bauder, 1986). The soil textural class was found using the USDA triangle method based on the results from the particle size analysis.

Estimation of the spatial distribution of soil thickness

We used several empirical models to estimate soil thickness based on the topographic features obtained from the 30 m ASTER elevation map. First, we applied the approach of Saulnier *et al*. (1997) that assumes a linear decrease between soil thickness and elevation (referred to here as the S-Z-97 method). In this approach, the soil depth (h_i) for pixel i is:

$$h_i = h_{max} - \left[\frac{z_i - z_{min}}{z_{max} - z_{min}}\right](h_{max} - h_{min}) \quad (1)$$

where z_i is the pixel elevation, z_{min} and z_{max} are the minimum and maxi-

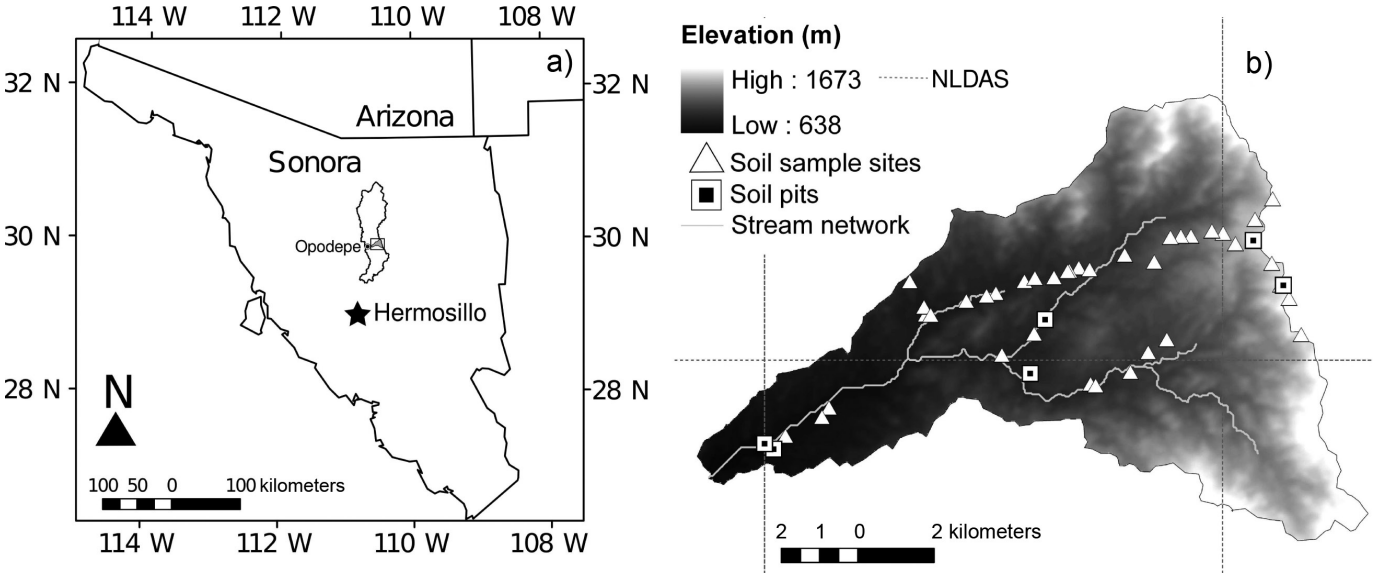

Figure 1. (a) Location of the Sierra Los Locos (SLL) watershed in the Rio San Miguel, Sonora, Mexico. (b) SLL elevation with the watershed boundary, stream network, field sites (soil pits and surface soil sampling sites) and the spatial extent of NLDAS-2 forcing fields.

mum elevations in the watershed and h_{min} and h_{max} are the minimum and maximum observed soil depths. Elevation values were extracted at the location of the soil pits from the 30 m ASTER digital elevation model while h_i was computed with ArcGIS 10.1 raster calculator. Saulnier *et al*. (1997) also developed an alternative method for soil depth estimation assuming a linear relation between soil thickness and terrain slope (referred to here as the S-S-97 method) as:

$$h_i = h_{max} - \left[1 - \frac{\tan\theta_i - \tan\theta_{min}}{\tan\theta_{max} - \tan\theta_{min}}\left(1 - \frac{h_{min}}{h_{max}}\right)\right] \quad (2)$$

where tan θ_i is the local calculated slope in degrees and tan θ_{min} and tan θ_{max} are the minimum and maximum slopes in the watershed. Terrain slope was calculated using ArcGIS 10.1 (Spatial Analyst) using the ASTER digital elevation model as input data, while soil depth (h_i) was estimated using the ArcGIS 10.1 raster calculator. Third, we implemented the approach of Gessler *et al*. (1995) to estimate the spatial distribution of soil thickness based on a multi-linear regression between curvature of the surface using the approach of Moore *et al*. (1993) , topographic index and soil depth (referred to here as the G-95 method). The topographic index (*TI*) in the watershed was obtained following the approach of Beven and Kirby (1979) as:

$$TI = \ln\left(\frac{CA}{\tan\theta}\right) \quad (3)$$

where *CA* is the upslope contributing area obtained following Jenson and Domingue (1988) and θ is the local slope angle. The topographic index, contributing area and the surface curvature were computed in ArcGIS 10.1. The multi-linear regression was performed to estimate soil depth by using 30 m pixel values of curvature (*CU*, defined as the combination of plan and profile curvature) and *TI* at the soil pit locations as independent variables. Finally, we evaluated a soil thickness estimation approach relying on the curvature distribution, regarded as a preferred way to infer soil depth from terrain attributes (*e.g*., Heimsath *et al*., 1999; Dietrich *et al*., 2003). The method of Heimsath *et al*. (1999, referred to here as the H-99 method) is based on a linear regression between surface curvature obtained using a fourth-order polynomial (Moore *et al*., 1993) at the soil pit locations and the measured soil thickness. Estimated soil thickness distributions were smoothed and resampled to a resolution of 120 m using a bilinear interpolation method to reduce differences between adjacent pixels and avoid unrealistic soil depth gradients. Terrain analyses and processing steps were carried out using ArcGIS 10.1.

Estimation of the spatial distribution of soil texture

We used several methods to obtain the spatial distribution of soil texture within the SLL basin. First, the soil texture map from the Instituto Nacional de Estadística y Geografía (referred to here as the INEGI method) provided a coarse representation of the major variations in soil properties within the watershed. While this product cannot capture high-resolution variations in soil texture, it serves as a benchmark that is considered as a standard in Mexico. Second, we employed the soil map derived by Vivoni *et al*. (2010) that is based on a combination of the INEGI map and a classification of terrain slope with some limited verification with the soil sampling conducted in the watershed. While this map exhibits a marked improvement in the soil texture distribution, it assumes an empirical distribution between particle size distribution and surface slope (referred to here as the Slope-based method). Finally, we employed an ASTER image obtained during the dry season (May 15, 2008) to determine surface soil texture based on the L1B registered radiance values (referred to here as the ASTER-based method) using methods described by Apan *et al*. (2002) and Liao *et al*. (2014). Digital numbers (DN) for different bands were converted to radiances through the use of a unit conversion coefficient. Bands represent the visible to near infrared region (bands 1 to 7 at 15 m resolution) and the thermal infrared (band 10 to 14 at 30 to 90 m resolution) region. The image acquisition in the dry season allowed for maximum exposure of the surface soils and minimized the effects of vegetation. We grouped radiance values into the four texture classes found in the SLL watershed: sandy clay loam, sandy loam, loamy sand and sand. The mean and standard deviation of the radiance values of each band were calculated for each soil class. The bands that showed significant differences in radiance values among textural classes were then selected for a subsequent image classification based on cluster analysis and a maximum likelihood unsupervised approach implemented in ArcGIS 10.1.

Evaluation of performance of spatially-distributed soil texture and depth maps

Performance of soil thickness model was evaluated with two different approaches. The first approach includes the estimation of mean absolute error (MAE) defined as:

$$MAE = \frac{1}{n}\sum_{i=1}^{n}\left|O_i - I_i\right| \quad (4)$$

where n is the number of observations, O_i is the observed soil thickness and I_i is the estimated soil thickness. The second approach included the computation of the Akaike Information Criterion (AIC) which is an analysis that allows selecting the best model among several ones based on the strength of evidence for each one. The model with the smallest AIC is regarded as the optimal one of all the proposed models. AIC is defined as:

$$AIC = n\log\left(\sigma^2\right) + 2k \quad (5)$$

where k is the number of estimated parameters in the model plus one and σ^2 is an estimate of the variance of residuals and is given by:

$$\sigma^2 = \frac{1}{n}\sum_{i=1}^{n}\left(O_i - I_i\right) \quad (6)$$

Furthermore, the delta AIC (Δ_i) is defined as the difference between the AIC of certain model (AIC_i) with the minimum AIC (AIC_{min}). This is a measure of each model relative to the best model, where the larger the AIC difference of a model, the less plausible it is to be the best one. Finally, the Akaike weights (w_i) represent the ratio of Δ_i values for each model relative to the whole set of R candidate models:

$$w_i = \frac{e^{(-\Delta_i/2)}}{\sum_{i=1}^{R} e^{(-\Delta_i/2)}} \quad (7)$$

The interpretation of Akaike weights is straightforward, they indicate the probability that the model is the best among the whole set of candidate models. The accuracy of soil texture maps was evaluated by the use of an error matrix that consists of extracting the soil texture category in the estimated map at the location of the 42 surface samples. Once extracted, the texture category of the map is compared with the observed texture in the field. The accuracy of the map is reported as the ratio of correct classified pixels to total number of extracted pixels (n = 42).

Hydrologic model description, meteorological forcing and parameterization

Numerical simulations of hydrologic conditions were carried out in the SLL watershed using the tRIBS model. The Triangulated Irregular Network (TIN) that represents the watershed terrain consists of elevation, stream network and boundary nodes with a reduced

number of model elements as compared to the original 30 m elevation field from ASTER (*e.g.*, Vivoni *et al.*, 2004). In the SLL watershed, the model is based on 49,390 Voronoi polygons that are the nearest neighborhood of each TIN node and used as a finite volume domain for water and energy calculations (Ivanov *et al.*, 2004). For each Voronoi polygon, the model accounts for a range of hydrologic processes in response to meteorological forcing, including: (1) canopy interception; (2) evapotranspiration from bare soil and vegetated surfaces; (3) infiltration and soil moisture redistribution; (4) shallow subsurface flow; and (5) overland and channel flow. In previous studies, tRIBS has shown good performance with respect to soil moisture, surface temperature and evapotranspiration data in the SLL watershed (Vivoni *et al.*, 2010; Mascaro and Vivoni, 2012; Méndez-Barroso *et al.*, 2014; Xiang *et al.*, 2014). Model simulations for the 2004 summer season (May 1 to September 30) were carried out using the parallel computing capabilities described by Vivoni *et al.* (2011) on 15 processors. The first month of simulation consisted of a dry period with no rainfall used as a model spin-up to deplete the initial soil moisture. The spin-up period was excluded from the model comparisons performed. During the simulation period, the meteorological forcing was based on ground-corrected grids obtained from the North American Land Data Assimilation System, version 2 (NLDAS-2), as described by Xiang *et al.* (2014). As shown in Figure 1b, the spatial resolution of the NLDAS-2 forcing fields (atmospheric pressure, relative humidity, incoming shortwave radiation, air temperature, wind speed and precipitation) was 12 km, leading to a few pixels over the SLL watershed (5 in total). In addition to the time-varying meteorological forcing, the simulations also accounted for the temporal variation of the vegetation conditions due to the rapid greenup occurring in the SLL watershed during the summer. This was achieved by developing empirical relations between remotely-sensed variables from the MODerate Resolution Imaging Spectrometer (MODIS) and vegetation parameters, as discussed in Méndez-Barroso et al. (2014). Albedo, Normalized Difference Vegetation Index (NDVI), Leaf Area Index (LAI) and the Fraction of Photosynthetically Active Radiation (FPAR), available at resolutions of 250 m to 1 km and repeat intervals of 8 to 16 days, were used to derive vegetation fields (vegetation fraction, stomatal resistance, maximum canopy storage, free throughfall coefficient, optical transmission coefficient and albedo) for the model.

Sensitivity analysis of soil thickness and soil texture distributions

To evaluate the effects of soil thickness and texture on the hydrologic conditions in the SLL watershed, we conducted simulations for identical model setups (*e.g.*, domain, initial state, meteorological forcing, vegetation variations), except for the specification of the soil property distributions. The simulation of Xiang *et al.* (2014) served as a benchmark case, where the Slope-based method for soil texture was used along with a uniform soil depth of 1.5 m. Given the excellent performance of the benchmark (B) case with respect to surface soil moisture, soil temperature and evapotranspiration measurements; it represents closely the hydrological conditions during the North American monsoon as reported in Xiang *et al.* (2014). Hence, the variation of the soil thickness and texture patterns performed here should be considered as a sensitivity analysis. We evaluated different combinations of soil depth and soil texture scenarios, as described in Table 1, for four spatially-variable soil depth maps (S-S-97, S-Z-97, G-95, H-99) and three spatially-variable soil texture maps (INEGI, Slope-based, ASTER-based), as well as two basin-wide uniform soil depths (1.0 and 1.5 m) and four basin-wide uniform textural classes (sand, sandy loam, sandy clay loam and loamy sand, with uniform soil depth of 1.5 m). As a result, a total of twenty-two different combinations of soil depth and texture were performed. In each simulation, the soil hydraulic properties for each soil texture class were kept identical, following Xiang *et al.* (2014), in such a way that the sensitivity analysis focused on the combined effects of the spatial patterns of soil thickness and texture. Xiang *et al.* (2014) obtained the initial soil

Table 1. Combinations of distributed soil depth and soil texture used in model simulations.

Simulation number	Soil thickness approach	Mean ± standard deviation of soil thickness (m9	Soil texture approach	Simulation ID
1	Uniform	1.5	Slope-based	B
2	Uniform	1.5	ASTER-based	UB+A
3	Uniform	1.5	INEGI	UB+I
4	Uniform	1.5	Sandy loam	UB+Sal
5	Uniform	1.5	Sand	UB+Sa
6	Uniform	1.5	Loamy sand	UB+lSa
7	Uniform	1.5	Sandy clay loam	UB+Sacl
8	G-95	0.80±0.46	Slope-based	G+S
9	H-99	0.83±0.50	Slope-based	H+S
10	S-S-97	1.53±0.28	Slope-based	S+S
11	S-Z-97	1.19±0.42	Slope-based	Z+S
12	G-95	0.80±0.46	ASTER-based	G+A
13	H-99	0.83±0.50	ASTER-based	H+A
14	S-S-97	1.53±0.28	ASTER-based	S+A
15	S-Z-97	1.19±0.42	ASTER-based	Z+A
16	G-95	0.80±0.46	INEGI	G+I
17	H-99	0.83±0.50	INEGI	H+I
18	S-S-97	1.53±0.28	INEGI	S+I
19	S-Z-97	1.19±0.42	INEGI	Z+I
20	Uniform	1.0±0.34	Slope-based	U+S
21	Uniform	1.0±0.34	ASTER-based	U+A
22	Uniform	1.0±0.34	INEGI	U+I

Table 2. Model parameters for soil classes in SLL watershed simulations (Xiang *et al.*, 2014).

Parameter	Variable (unit)	Rock	Sand	Loamy sand	Sandy loam	Sandy clay loam
Saturated hydraulic conductivity	K_s (mm/h)	25	1,662	598	241	98
Saturated soil moisture content	θ_s (-)	0.285	0.317	0.301	0.310	0.230
Residual soil moisture content	θ_r (-)	0.009	0.010	0.005	0.015	0.058
Pore size distribution index	m (-)	0.17	0.60	0.45	1.50	0.32
Air entry bubbling pressure	ψ_b (mm)	0	0	0	0	0
Conductivity decay parameter	f (mm^{-1})	0.01	0.01	0.025	0.001	0.001
Conductivity anisotropy ratio	A_s (-)	600	600	600	600	600
Soil porosity	n (-)	0.385	0.437	0.437	0.453	0.398
Dry soil heat conductivity Wet soil heat conductivity	k_s (J/msK)	1.2 1.3	1.2 1.3	1.2 1.3	1.2 1.3	1.2 1.3
Dry soil heat capacity Wet soil heat capacity	C_s (J/m^3K)	$6x10^5$ $1.3x10^6$	$6x10^5$ $1.3x10^6$	$6x10^5$ $1.3x10^6$	$6x10^5$ $1.3x10^6$	$6x10^5$ $1.3x10^6$

parameters from soil pedotransfer functions based on particle size fraction and bulk density (Van Genuchten, 1980; Rawls *et al.*, 1983; Rawls and Brakensiek, 1989) followed by manual calibration. Table 2 presents the soil parameter values for the tRIBS model used for each of the texture classes.

RESULTS AND DISCUSSION

Evaluation of distributed soil thickness and soil texture approaches

prior to discussing the effects of soil thickness and texture on the hydrologic response of the SLL watershed, we evaluate each approach with respect to the field observations. Figure 2 compares the spatial distribution of soil thickness derived from each method along with the resulting basin-averaged soil depth ($\overline{h}$) and its spatial standard deviation (σ_h), while Table 3 presents the absolute errors (cm) at the soil pit locations. Lower absolute errors and lower basin-averaged depths are apparent for the G-95 (0.80±0.46 m) and H-99 (0.83±0.53 m) methods that were tailored to the study watershed through local regressions using the soil pit observations. The G-95 method resulted in $h_i = 37.12+3.31TI_i-242.19CU_i+598TI_iCU_i$ (cm), where CU_i is the curvature of pixel i at 30 m resolution (1/100 m), yielding a relation with an $R^2=0.77$ ($p < 0.01$) and an absolute error of 11.6 cm. Similarly, the H-99 method resulted in a relationship of the form $h_i=-198.82CU_i+79.9$ (cm), with an $R^2=0.71$ ($p < 0.01$) and an absolute error of 15.5 cm. In contrast, the S-Z-97 (1.19±0.42 m) and the S-S-97 (1.53±0.28 m) methods resulted in higher basin-averaged soil depths and larger errors as compared to the field observations (Table 3). The

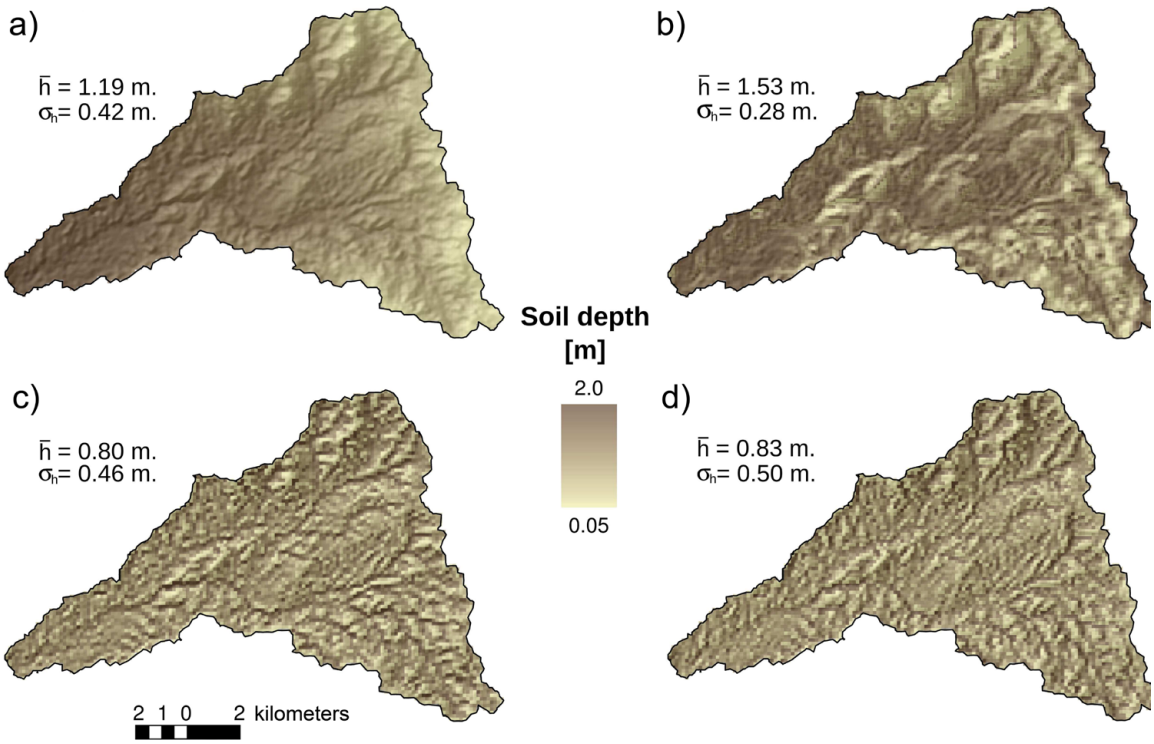

Figure 2. Comparison of soil thickness distributions for (a) S-Z-97, (b) S-S-97, (c) G-95 and (d) H-99 methods. The basin-averaged soil depth and the spatial standard deviations are shown.

Table 3. Accuracy of soil thickness and texture approaches at soil pit and surface sampling sites. The absolute error is the mean at the saoil pit locations.

Soil thickness approach	**Absolute error** (cm)
S-Z-97	38.4
S-S-97	92.4
G-95	11.6
H-99	15.5
Soil texture approach	**Correct pixels** (%)
INEGI	53
Slope-based	56
ASTER-based	68

spatial distributions reveal a smoother variation in the S-Z-97 and S-S-97 methods that closely mimic the elevation or slope variations in the SLL watershed, while the G-95 and H-99 approaches exhibit more dramatic differences associated with the curvature (G-95 and H-99) and topographic index (G-95) distributions, which tend to be more complex (Vivoni *et al*., 2004). From a geomorphologic perspective, the methods that account for terrain curvature (G-95 and H-99) are more appealing since these capture the shallow soils observed near mountain ridges and the deeper soils in valley bottoms where material is accumulated from depositional processes.

The second approach to measure the selection of the "best model" with the application of the Akaike Information Criterion (AIC) is shown in Table 4 and provides consistent results to the prior analyses. The H-99 method resulted in the best model for soil depth estimation in the SLL basin, leading to the smallest AIC among the evaluated models (16.36), while the Akaike weight (w_i) indicated a probability of 63% of being the best model. The G-95 method also exhibited a good performance, due to its relatively low AIC and Δ_i. However, a relatively low value of w_i (37% of being the best model) indicates this model is not as good as the H-99 method at this site. Thus, the two approaches used to assess the best method for soil depth estimation yielded consistent outcomes. Nevertheless, the main goal of this study is to evaluate the effect of different soil depth and texture distributions on controlling basin water fluxes and states.

Figure 3 presents the comparison of the soil texture distributions for the three different methods, while Table 3 indicates the percentages of correctly classified pixels as compared to the surface soil samples (extracted pixels on the location of the 42 surface samples collected in the basin). The official soil map from INEGI has three soil classes with a clear pattern of finer soils at higher elevations (sandy loam) and coarser soils at lower elevations (sand), with 53% of pixels at sampling sites correctly classified. Accounting for surface slope, as performed by Vivoni *et al*. (2010), improved the classification accuracy to 56%, while also adding rock outcrops at the highest slope sites and sandy clay loam areas near the floodplain zones. The use of the ASTER visible and thermal bands showed clear spatial differences in radiances that were associated to surface soil features. For example, for bands 1 (green), 2 (red) and 3 (near infrared), a clear distinction was achieved between areas with sand and sandy loam soils, while thermal bands (12 and 13) helped to distinguish loamy sand and sand regions. As a result, the ASTER-based map shows some of the general characteristics of the other approaches with respect to the variation with elevation, but more clearly distinguishes the soil texture classes, including rock outcrops. From a geological perspective, the soil texture variations appear more realistic and achieve an improved accuracy of 68% as compared to the surface soil sampling sites.

Table 4b Results of the Akaike Information Criterion (AIC) for the models used to estimate spatially-distributed soil depth. In addition to the AIC, the difference to smallest AIC (Δ_i), and the Akaike weight (w_i) were estimated.

Model	**AIC**	Δ_i	**Exp(-Δi/2)**	w_i
H-99	16.36	0.00	1.0000	0.63
G-95	17.45	1.09	0.5809	0.37
S-Z-97	28.97	12.61	0.0018	0.00
S-S-97	32.01	15.65	0.0004	0.00

Comparisons of basin-averaged water balance components to data for benchmark case

Given the importance of establishing confidence in the model simulations, we next present a comparison to the available field observations during SMEX04 (Vivoni *et al*., 2007a, 2008b; Ryu *et al*., 2010). Figure 4 shows the basin-averaged water balance components for the benchmark (B) simulation using a uniform soil thickness of 1.5 m and the Slope-based texture map, as in Xiang *et al*. (2014). The rainfall amounts and their distribution in time dictate the hydrologic responses in terms of soil moisture (SM), evapotranspiration (ET), streamflow (Q) and the change in the depth to the groundwater table (N_{wt}). With sufficient rainfall during the summer season, vegetation communities in the SLL watershed increase in greenness (NDVI) through leaf production (Vivoni, 2012). The temporal evolution of surface soil moisture (5 cm depth average SM) and root zone soil moisture (1 m depth average SM) illustrate well how the dry conditions prior to the NAM substantially change upon the arrival of rainfall events. In addition, the benchmark simulation captures a soil moisture recession period in August that is present in ground data (Vivoni *et al*., 2008b) and within a remotely-sensed product (2D-STAR, Ryu *et al*., 2010), providing confidence in the simulated surface soil moisture dynamics.

As the NAM season begins in late June, basin-averaged conditions moisten considerably, as shown by higher SM in the surface soil and root zones, a shallower N_{wt}, a higher ET and the production of runoff that is observed as Q at the basin outlet. Initially, the hydrologic response is of a pulsed nature due to the dry conditions prior to the NAM and the short duration of the first rainfall events. Nevertheless, the long sequence of consecutive storms in July lead to a system that is seasonally-wet with steady amounts of SM, ET and Q. This behavior is interrupted by a long dry period in August with a decrease in SM, a stabilization of N_{wt}, a sharp reduction of Q and a small decrease in ET. These dry-down conditions due to the absence of rainfall events were also reflected in the vegetation response within the basin where the basin-averaged NDVI slightly decreased and stabilized (Vivoni, 2012). Continuous water losses to evapotranspiration in the watershed eventually lead to drier conditions in the surface soils and root zone. As this hydrologic process is taking place, the lateral redistribution of water through hillslopes results in a downstream shift of soil moisture towards valley bottoms (Vivoni *et al*., 2007a). Overall, we would expect that the spatial distribution of hydrologic states and fluxes during the wetting and drying cycles should depend on the patterns of soil thickness and texture as these have a control on the ability of a soil to store and transmit water to evapotranspiration and lateral redistribution.

Sensitivity of basin-averaged ET and runoff to soil thickness and texture

We evaluated the twenty-two simulations representing different soil thickness and texture distributions (Table 1) with respect to the major

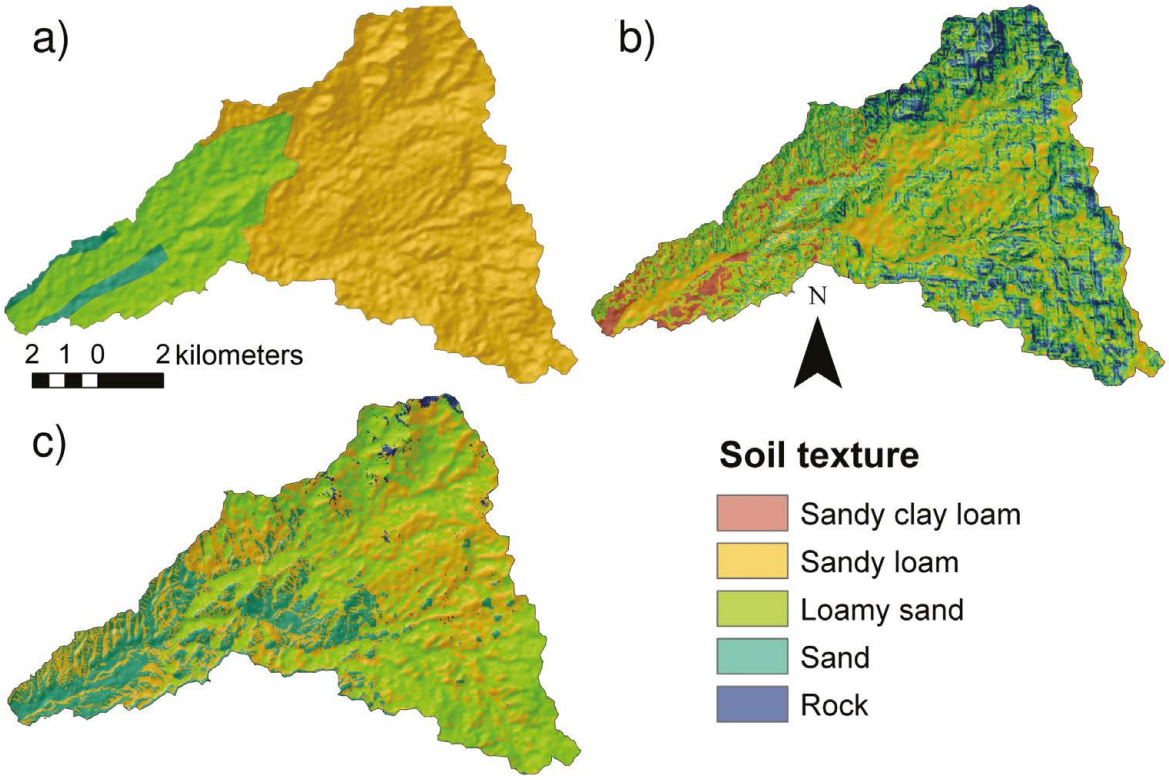

Figure 3. Comparison of soil texture distributions from (a) INEGI, (b) Slope-based method and (c) ASTER-based method with the corresponding textural classes described in Table 2.

water losses in the SLL watershed, specifically the basin-averaged ET and runoff. Figure 5 presents the cumulative water losses (mm) during the 2004 summer season (June 1 to September 30) for seventeen of the cases, selected to represent the full range of simulated conditions. Two cases with uniform soil texture (UB+Sa, UB+lSa) and three cases with shallow, uniform soil thickness (U+I, U+S, U+A) were excluded due to similarities to other results. Basin-averaged ET (Figure 5a) showed a range of ~100 mm among the cases when accumulated over the study period with the uniform soil texture simulations defining the upper (UB+Sacl, sandy clay loam) and lower bounds (UB+Sal, sandy loam). This indicates that soil texture exhibited a stronger control than soil thickness on the basin-averaged ET magnitudes, as expected from the effects of particle size on infiltration and water retention in soils (*e.g.*, Noy-Meir, 1973; Sala *et al*., 1988; Rodriguez-Iturbe *et al*., 1999; English *et al*., 2005). Soils with finer fractions (sandy clay loam) have more water availability, which enhances ET as compared to coarser soils (sandy loam). In a similar fashion, the soil thickness distributions that promoted higher water availability associated with spatial gradients in terrain curvature (*CU*) and in topographic index (*TI*), such as H+S and G+S, also had greater ET accumulations over the season. Different combinations of soil thickness and texture maps could yield either seasonal ET amounts that exceeded or were less than the benchmark (B) case.

Figure 6 shows this through a subset of simulations where either the soil thickness (Z+S, S+S, H+S, G+S) or the soil texture was varied (UB+Sal, UB+Sacl, UB+Sa, UB+lSa, UB+I, UB+A), while the other factor was kept constant. The bias (or percent difference) of the basin-averaged ET between each simulation and the benchmark is shown. Basin-averaged ET was consistently larger in the soil thickness simulations as compared to the benchmark case with a uniform 1.5 m soil depth, indicating that spatially variable soil depths lead to higher wetness. We also found that the differences between the soil thickness cases and the benchmark were statistically significant (t-test analysis) for the basin-averaged ET for three of the four cases (Table 5). In contrast, the soil texture simulations might have higher or lower ET than the benchmark case, depending on the dominance of coarse (sand) or fine (sandy clay loam) texture.

Runoff losses shown in Figure 5 are separated into surface runoff (infiltration-excess and saturation-excess runoff, Figure 5b) and groundwater runoff (perched return flow and groundwater exfiltration, Figure 5c) mechanisms (Ivanov *et al*., 2004; Vivoni *et al*., 2007b). The specification of soil texture and thickness distributions has a marked impact on cumulative runoff, in particular for the groundwater component. In most simulations, the benchmark case exhibited lower cumulative surface and groundwater runoff, indicating that both soil texture and thickness play an important role. For the soil thickness distributions that involved spatial gradients in *CU* and *TI* (*e.g.*, G+I, H+I), the sharp changes in the soil depth caused significant increases in groundwater runoff. This is consistent with work on the role played by the soil-bedrock interface on lateral soil water redistribution and subsurface runoff production (*e.g.*, Tromp-Van Meerveld and McDonnell, 2006; Weiler and McDonnell, 2006; Lanni *et al*., 2013). In particular, depressions in the soil-bedrock interface, observed here as thicker soils, can sustain wetter soil conditions through a temporarily perched groundwater table and act as impedance for downslope drainage (Lanni *et al*., 2013). This was corroborated by differences between the soil thickness distributions and the benchmark case (Table 5), where the three approaches with large spatial variability (S-S-97, G-95, H-99) resulted in highly statistically significant differences of streamflow at the basin outlet, whereas the smoothly-varying case (S-Z-97) was indistinguishable from a uniform soil depth.

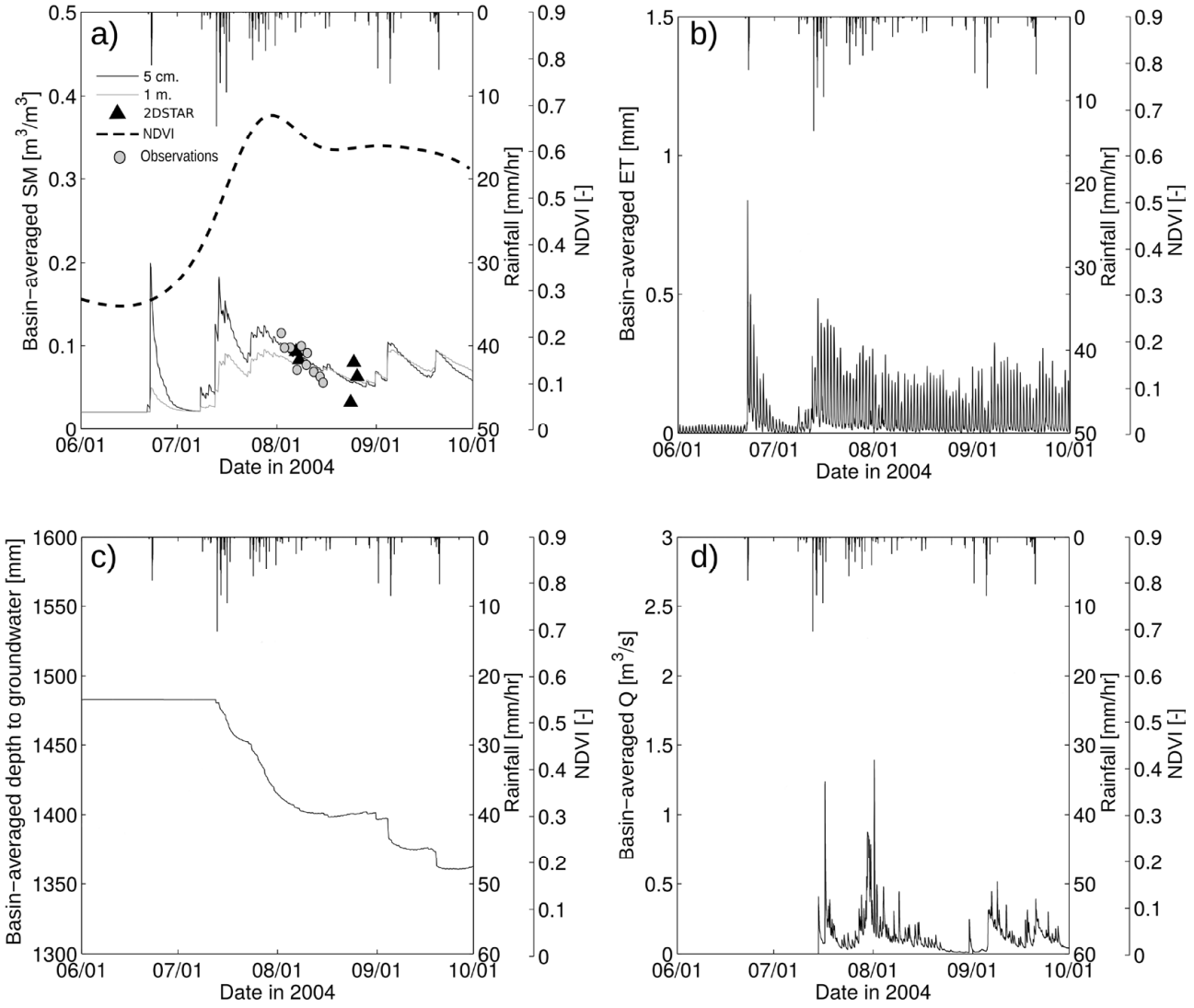

Figure 4. Basin-averaged water balance components during study period (after 1 month spin-up, June 1 to September 30, 2004). (a) Volumetric soil moisture (SM, m^3/m^3) for 5-cm and 1-m depth averages as compared to remotely-sensed 2D-STAR product and ground observations. (b) Evapotranspiration (ET, mm/hr). (c) Depth to the groundwater table (N_{wt}, mm). (d) Streamflow at the basin outlet (Q, m^3/s). Basin-averaged NDVI and rainfall (mm/hr) are shown in all panels.

Spatial patterns of surface soil moisture and evapotranspiration

Next, we evaluated the role of spatially-variable soil thickness and soil texture on the spatial patterns of surface soil moisture (top 5 cm, SM) and evapotranspiration. Three soil thickness and two soil texture distributions were selected for comparison to the benchmark simulation: (1) the soil thickness cases had contrasting spatial distributions (G-95, S-Z-97, uniform at 1.5 m) and (2) the soil texture maps represented the more realistic cases (Slope-based, ASTER-based). Figure 7 presents spatial maps of surface SM, expressed in dimensionless units as degree of saturation (volumetric SM divided by soil porosity), for the benchmark, G+S, Z+S and UB+A cases. Simulations that shared the same soil texture map (Slope-based in benchmark, G+S, Z+S) exhibited similar patterns of time-averaged surface SM. Wetter conditions were found in sandy clay loam soils in floodplain areas, moderately wet conditions matched sandy loam locations, and sand and loamy sand soils were drier sites in the watershed. Nevertheless, the range of soil moisture varied considerably among these cases due to the effect of the soil thickness distributions. For example, the G+S simulation exhibited high relative SM values due to the effect of the varying soil depth on soil water accumulation within depressions at the soil-bedrock interface. In contrast, the simulation with a different soil texture map based on ASTER (UB+A) exhibited surface SM patterns that varied widely from the other cases. Here, the low amounts of areas with sandy clay loam limit the occurrence of wet soils and the spatial differences closely follow the soil texture map. For a uniform soil depth, comparison of the benchmark and UB+A cases demonstrates the strong overriding control of surface soil texture on the relative SM within shallow soil layers.

Figure 8 compares the spatial patterns of seasonal ET (mm) accumulated during the study period for the benchmark, G+S, Z+S and UB+A cases. A detailed comparison between the benchmark, G+S and Z+S cases (similar Slope-based method for soil texture, different soil thickness distributions) reveals that soil thickness has a very distinct impact on ET. High seasonal ET values are observed in locations with thinner soils which coincide with high elevations for the Z+S approach and with ridges for the G+S approach. Soil texture distributions also

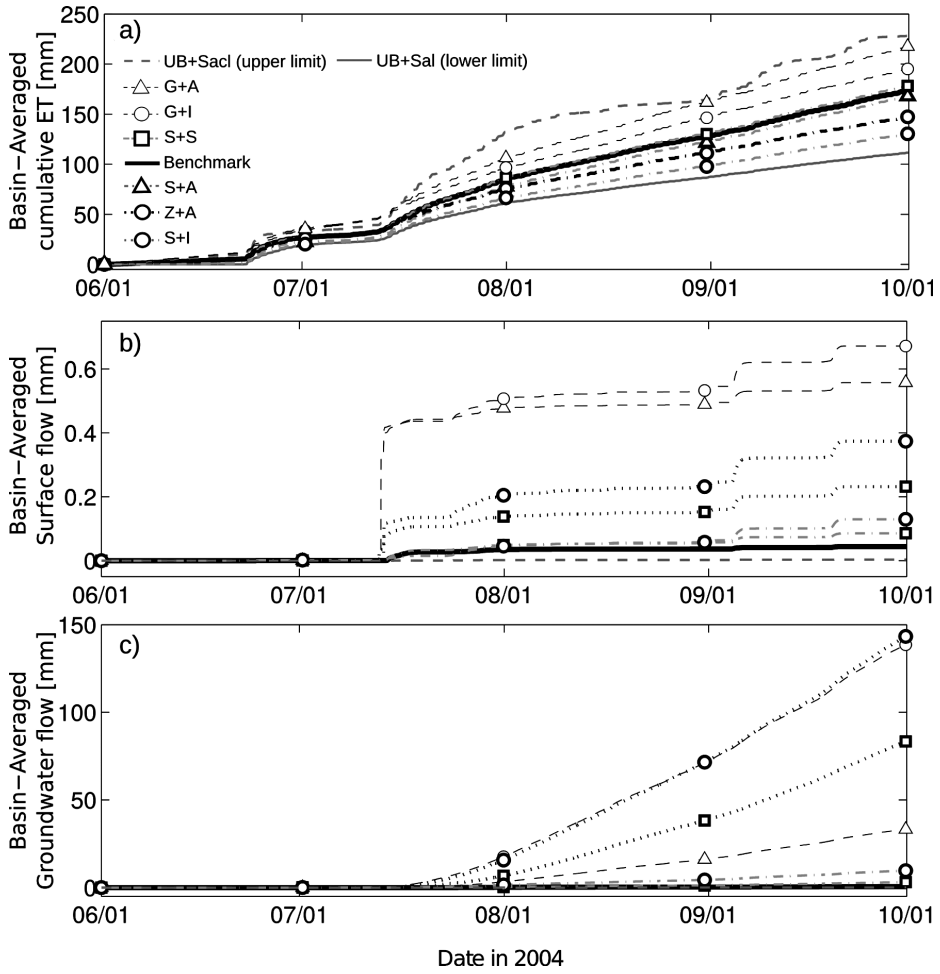

Figure 5. Basin-averaged cumulative water losses for a subset of the simulations which include: UB+Sal (1.5 m soil thickness + uniform sandy loam soil), UB+Sacl (1.5 m soil thickness + uniform sandy clay loam), G+A (variable soil thickness G-95 + ASTER-based texture), G+I (variable soil thickness G-95 + INEGI-based texture), S+S (variable soil thickness SS-97 + slope-based texture), model benchmark (Xiang et al., 2014), S+A (variable soil thickness SS-97 + ASTER-based texture), Z+A (variable soil thickness SZ-97 + ASTER-based texture), and S+I (variable soil thickness SS-97 + INEGI-based texture). (a) Evapotranspiration (ET, mm). (b) Surface runoff (mm). (c) Groundwater runoff (mm).

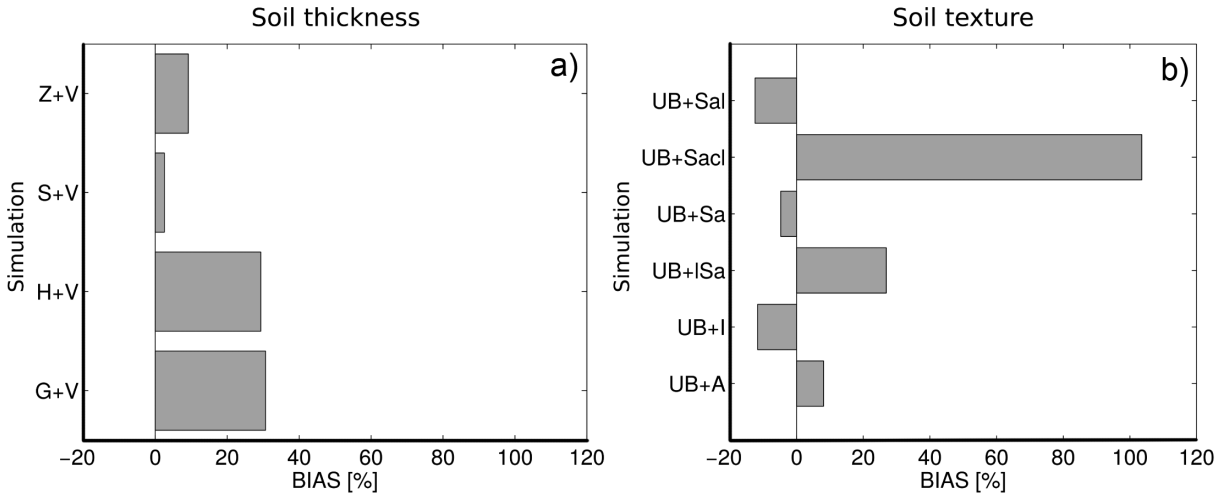

Figure 6. Bias (%) between each simulation and benchmark for basin-averaged evapotranspiration. (a) Simulations with different soil thickness and same soil texture. (b) Simulations with different soil texture and same soil thickness. Table 1 defines the simulation IDs.

Table 5. Results of t-test evaluating the statistical significance of the differences between evapotranspiration (ET) and streamflow (Q) simulated by varying the soil thickness and the ET and Q simulated by the benchmark case. p-values are reported along with the statistical significance indicated as highly significant (****), significant (**) and not significant (-).

Soil thickness approach	ET		Q	
	p	Significance	p	Significance
S-Z-97	0.01	**	0.254	NS
S-S-97	0.41	NS	< 0.001	****
G-95	< 0.001	****	< 0.001	****
H-99	< 0.001	****	< 0.001	****

matter as there is a substantial difference in seasonal ET between the two uniform soil thickness cases (benchmark, UB+A), with a lower amount of ET for the case with coarser soils (UB+A). Clearly, there is a complex interplay at work between the soil thickness and soil texture distributions that lead to a wide range of spatial patterns within the SLL basin on seasonal surface soil moisture and evapotranspiration.

SUMMARY AND CONCLUSIONS

Assessing the spatial controls on the hydrologic response of semiarid watersheds is important for determining the level of detail required in the representations of terrain, vegetation and soil conditions used in process-based hydrologic models. While it is well known that specifying accurate soil depth and texture maps in distributed hydrologic models are important, these are some of the highest sources of uncertainty currently present in the hydrologic modeling process. Thus, advances in digital soil mapping through either terrain analyses or remotely-sensed indices are an important avenue of research activities. In this study, we derived a range of soil thickness and texture distributions using local terrain attributes, remotely-sensed radiance values and ground-based observations to obtain a set of plausible modeling scenarios for evaluating the sensitivity of the watershed response. We selected the Sierra Los Locos (SLL) watershed in northwest Mexico due to our prior efforts with the tRIBS distributed hydrologic model in this basin and the field observations that suggested a strong spatial variability in soil thickness and soil texture associated with terrain conditions.

The sensitivity analysis conducted with the various combinations of soil thickness and texture patterns revealed a strong sensitivity of the surface soil moisture, evapotranspiration and runoff in terms of their seasonal magnitudes and spatial distributions. Based on the evaluations with respect to the field samples (*e.g.*, soil pits and surface soil samples), we determined that the remotely-sensed soil texture map (ASTER-based) and the soil depth patterns using curvature and/or topographic index (G-95, H-99) were superior to other methods. Thus, a focus was placed on comparing different combinations that accounted for these improved products in light of the demonstrated model performance for the benchmark case. We found that the role played by soil thickness was related to the creation of spatial gradients (*e.g.*, depressions at the soil-bedrock interface) that affected the accumulation of soil water, its consumption by evapotranspiration and the generation of subsurface runoff. The filling and spilling of soil depressions was particularly important when the downstream locations had shallow soils. The role of soil texture was to set the baseline conditions for soil moisture patterns which impacted the generation of surface and groundwater runoff and the evapotranspiration process. In this seasonally wet system, we also identified that the influence of soil texture decreases in time, while the spatial control of soil thickness becomes more important in determining the spatial variations of soil moisture and evapotranspiration. Other semiarid watersheds in northwest Mexico are thus expected to be more sensitive to the spatial distribution of soil texture prior to the NAM and to the terrain-mediated patterns of soil depth during the progression of the monsoon season.

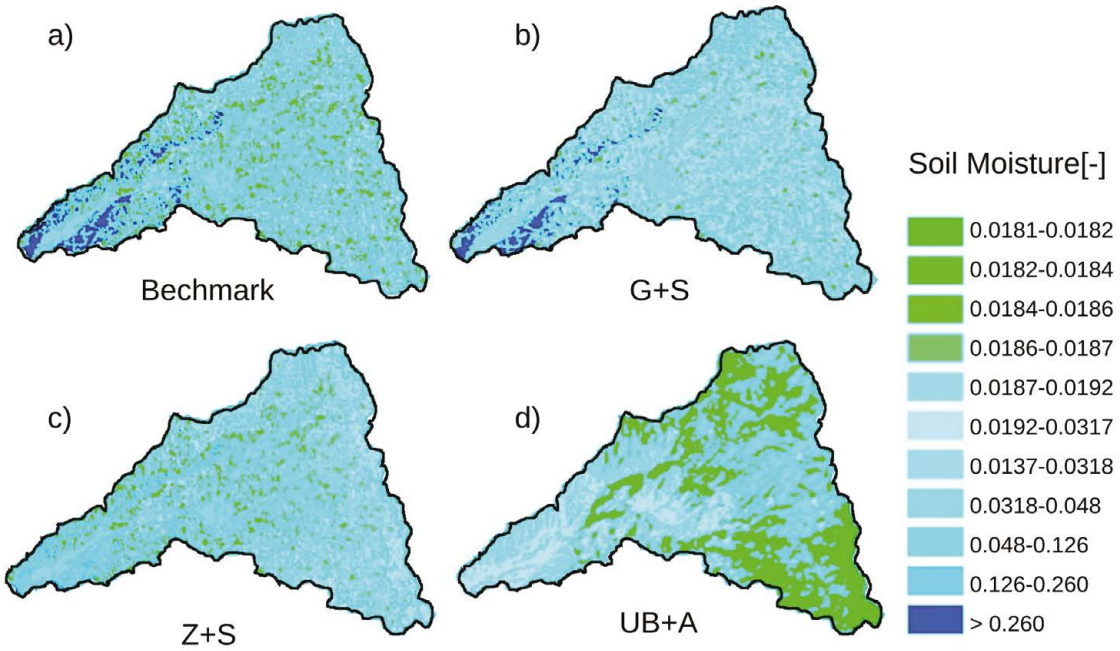

Figure 7. Comparison of selected simulations of relative surface soil moisture (SM, dimensionless, top 5-cm) for the benchmark (a), G+S (b), Z+S (c) and UB+A (d) cases. The maps represent the time-averaged soil moisture during the study period (June 1 to September 30, 2004).

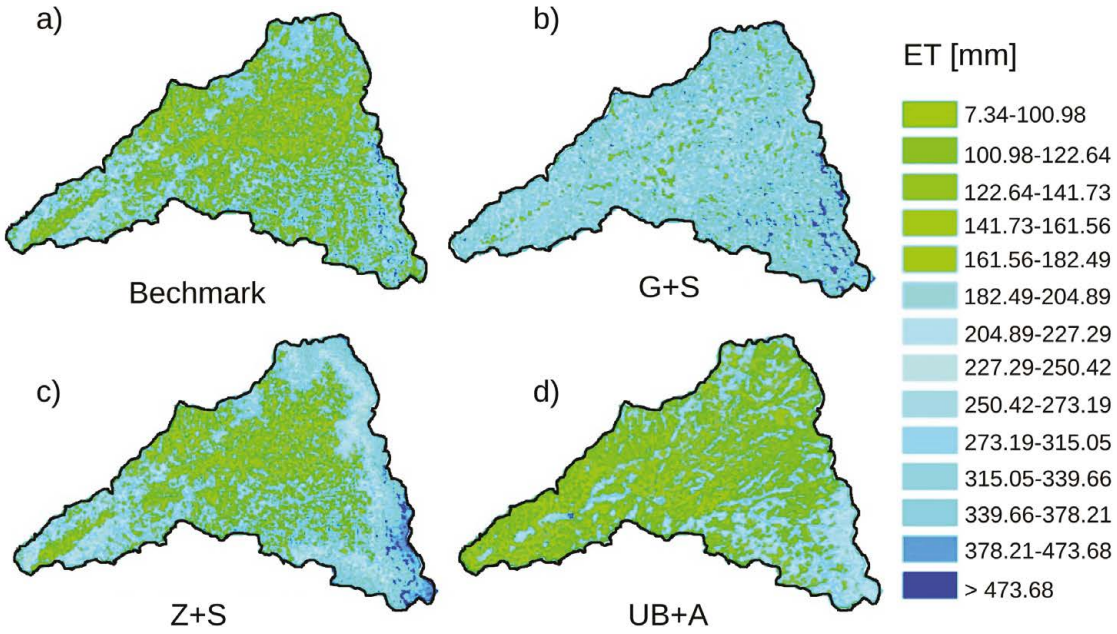

Figure 8. Comparison of selected simulations of evapotranspiration (ET, mm) for the benchmark (a), G+S (b), Z+S (c) and UB+A (d) cases. The maps represent the accumulated seasonal evapotranspiration during the study period (June 1 to September 30, 2004).

ACKNOWLEDGEMENTS

We acknowledge funding from the NOAA Climate Program Office (GC07–019), NSF IRES Program (OISE 0553852) and a Consejo Nacional de Ciencia y Tecnología (CONACyT) fellowship to the first author. The USDA-ARS SMEX04 project provided an important impetus for field observations and modeling activities in the region. We thank Christopher J. Watts and Julio C. Rodríguez for support in the field efforts. We also appreciate the discussion with Arjun Heimsath, Philip Christensen and Kelin Whipple on the methods utilized in the study.

REFERENCES

Apan, A., Jensen, T., Kelly, R., Strong, W., Butler, D., Basnet, B., 2002, Spectral Discrimination and Separability Analysis of Agricultural Crops, Soil Types, and Related Land Cover Using ASTER Imagery, Proceedings of the 11th Australasian Remote Sensing and Photogrammetry Conference, Brisbane, 2-6 September 2002, pp. 396-411.

Bertoldi, G., Rigon, R., Over, T.M., 2006, Impact of watershed geomorphic characteristics on the energy and water budgets: Journal of Hydrometeorology, 7, 389-403.

Beven, K.J., Kirby, M.J., 1979, A physically based variable contributing area model of basin hydrology: Hydrological Sciences Bulletin, 24, 43-69.

Beven, 2012

Blake, G.R., 1965, Bulk density, *in* Black, C.A. (ed.), Methods of Soil Analysis Part 1, Madison, Agronomy Monograph, 374-390.

Catani, F., Segoni, S., Falorni, G., 2010, An empirical geomorphology-based approach to the spatial prediction of soil thickness at catchment scale: Water Resources Research, 46: W05508. DOI:10.1029/2008WR007450.

Cuo, L., Giambelluca, T.W., Ziegler, A.D., 2011, Lumped parameter sensitivity analysis of a distributed hydrological model within tropical and temperate catchments: Hydrological Processes, 25, 2405-2421.

Dietrich, W., Bellugi, D., Sklar, L., Stock, J., Heimsath, A., Roering, J., 2003, Geomorphic transport laws for predicting landscape form and dynamics. *in* Wilcox, P., Iverson, S. (eds.), Prediction in Geomorphology: Washington, D.C., American Geophysical Union, Geophysical Monograph Series, 135, 103-132.

Dominguez, F., Kumar, P., Vivoni, E.R., 2008, Precipitation recycling variability and ecoclimatological stability - A study using NARR data, Part II: North American monsoon region: Journal of Climate, 21(20), 5187-5203.

English, N.B., Weltzin, J.F., Fravolini, A., Thomas, L., Williams, D.G., 2005, The influence of soil texture and vegetation on soil moisture under rainout shelters in a semidesert grassland: Journal of Arid Environments, 63, 324-343.

Fatichi, S., Vivoni, E.R., Ogden, F.L., Ivanov, V., Mirus, B., Gochis., D., Downer, C., Camporese, M., Davison, J.H., Ebel, B., Jones, N., Kim, J., Mascaro, G., Niswonger, R., Restrepo, P., Rigon, R., Shen, C., Sulis, M., Tarboton, D., 2016, An overview of current applications, challenges and future trends in distributed process-based models in hydrology: Journal of Hydrology, 537, 45-60.

Forzieri, G., Castelli, F., Vivoni, E.R., 2011, Vegetation dynamics within the North American monsoon region. Journal of Climate, 24(6), 1763-1783.

Forzieri, G., Feyen, L., Cescatti, A., Vivoni, E.R., 2014, Spatial and temporal variations in ecosystem response to monsoon precipitation variability in southwestern North America: Journal of Geophysical Research Biogeosciences, 119(10), 1999-2017 .

Garambois, P.A., Roux, H., Larnier, K., Castaings, W., Dartus, D., 2013, Characterization of process-oriented hydrological model behavior with temporal sensitivity analysis for flash floods in Mediterranean catchments: Hydrology and Earth System Sciences, 17, 2305-2322.

Gee, G.W., Bauder, J.W., 1986, Particle-size analysis. *in* A Klute (ed.) Methods of Soil Analysis, Part 1. Physical and Mineralogical Methods. Agronomy Monograph No. 9 (2ed): Madison, WI, American Society of Agronomy/ Soil Science Society of America, 383-411.

Gessler, P.E., Moore, I.D., McKenzie, N.J., Ryan, P., 1995, Soil-landscape modeling and spatial prediction of soil attributes: International Journal of Geographical Information Systems, 9(4), 421-432.

Gochis, D.J., Vivoni, E.R., Watts, C.J., 2010, The impact of soil depth on land surface energy and water fluxes in the North American Monsoon region: Journal of Arid Environments, 74, 564-571.

Heimsath, A.M., Dietrich, W.E., Nishiizumi, K., Finkel, R.C., 1999, Cosmogenic nuclides, topography, and the spatial variation of soil depth: Geomorphology, 27, 151-172.

Ivanov, V.Y., Vivoni, E.R., Bras, R.L., Entekhabi, D., 2004, Catchment hydrologic response with a fully-distributed triangulated irregular network model: Water Resources Research, 40(11), W11102, DOI:10.1029/2004WR003218.

Jenson, K.S., Domingue, J.O., 1988, Extracting topographic structure from digital elevation data for geographic information system analysis: Photogrammetric Engineering and Remote Sensing, 54(11), 1593-1600.

Lanni, C., McDonnell, J., Hopp, L., Rigon, R., 2013, Simulated effect of soil depth and bedrock topography on near-surface hydrologic response and slope stability: Earth Surface Processes and Landforms, 38, 146-159.

Liao, K., Xu, S., Wu, J., Zhu, Q., 2014, Spatial estimation of surface soil texture using remote sensing data: Soil Science and Plant Nutrition, 59(4), 488-500.

Mahmood, T.H., Vivoni, E.R., 2011, A climate-induced threshold in hydrologic response in a semiarid ponderosa pine hillslope: Water Resources Research, 47, W09529, DOI:10.1029/2011WR010384.

Mascaro, G., Vivoni, E.R., 2012, Utility of coarse and downscaled soil moisture products at L-band for hydrologic modeling at the catchment scale: Geophysical Research Letters, 39, L10403, DOI:10.1029/2012GL051809.

Mascaro, G., Vivoni, E.R., Gochis, D.J., Watts, C.J., Rodriguez, J.C., 2014, Temporal downscaling and statistical analysis of rainfall across a topographic transect in northwest Mexico: Journal of Applied Meteorology and Climatology, 53(4), 910-927.

Méndez-Barroso, L.A., Vivoni, E.R., Watts, C.J., Rodríguez, J.C., 2009, Seasonal and interannual relation between precipitation, surface soil moisture and vegetation dynamics in the North American monsoon region: Journal of Hydrology, 377, 59-70.

Méndez-Barroso, L.A., Vivoni, E.R., 2010, Observed shifts in land surface conditions during the North American monsoon: Implications for a vegetation-rainfall feedback mechanism: Journal of Arid Environments, 74(5), 549-555.

Méndez-Barroso, L.A., Vivoni, E.R., Robles-Morúa, A., Mascaro, G., Yépez, E.A., Rodriguez, J.C., Watts, C.J., Garatuza-Payan, J., Saiz-Hernandez, J.A., 2014, A modeling approach reveals differences in evapotranspiration and its partitioning in two semiarid ecosystems in Northwest Mexico: Water Resources Research, 50, 3229-3252.

Moore, I.D., Gessler, P.E., Nielsen, G.A., Petersen, G.A., 1993, Soil attribute prediction using terrain analysis: Soil Science Society of America Journal, 57, 443-452.

Nicótina, L., Tarboton, D.G., Tesfa, T.K., Rinaldo, A., 2011, Hydrologic controls on equilibrium soil depths: Water Resources Research, 47, W04517, DOI:10.1029/2010WR009538.

Noy-Meir, I., 1973, Desert Ecosystems: Environment and Producers: Annual Review of Ecology and Systematics, 4, 25-51.

Pelletier, J.D., Rasmussen, C., 2009, Geomorphically-based predictive mapping of soil thickness in upland watersheds: Water Resources Research, 45, W09417, DOI:10.1029/2008WR007319.

Rahimy, P., 2012, Effects of soil depth spatial variation on runoff simulation, using the Limburg soil erosion model (LISEM), a case study in Faucon catchment, France: Soil and Water Research, 2, 52-63.

Rawls, W.J., Brakensiek, D.L., Miller, N., 1983, Green-Ampt infiltration parameters from soils data, Journal of Hydraulic Engineering, 109(1), 62–70.

Rawls, W.J., Brakensiek, D.L., 1989, Estimation of soil water retention and hydraulic properties, *in* Morel-Seytoux, H.J. (ed.), Unsaturated Flow in Hydrologic Modeling: Theory and Practice: Dordrecht, Netherlands, Kluwer Academic Publishers, 275-300.

Robles-Morúa, A., Vivoni, E.R., Mayer, A., 2012, Distributed hydrologic modeling in northwest Mexico reveals the links between runoff mechanisms and evapotranspiration: Journal of Hydrometeorology, 13, 785-807.

Rodriguez-Iturbe, I., Porporato, A., Ridolfi, L., Isham, V., Cox, D., 1999, Probabilistic modelling of water balance at a point: The role of climate soil and vegetation, Proceedings of the Royal Sciety of London, Series A, 3789-3805.

Ryu, D., Jackson, T.J., Bindlish, R., Le Vine D.M., Hacken, M., 2010, Soil moisture retrieval using a two-dimensional L-band synthetic aperture radiometer in a semiarid environment: IEEE Transactions on Geoscience and Remote Sensing, 48(12), 4273-4283.

Sala, O.E., Parton, W.J., Lauenroth, W.K., Joyce, L.A., 1988, Primary production of the central grasslands region of the United States: Ecology, 69, 40-45.

Saulnier, G.M., Beven, K., Obled, C., 1997, Including spatially variable effective soil depths in TOPMODEL: Journal of Hydrology, 202, 158-172.

Singh, V., Woolhiser, D.A., 2002, Mathematical Modeling of watershed hydrology: Journal of Hydrological Engineering, 7(4), 270-284.

Sullivan, D.G., Shaw, N.J., Rickman, D., 2005, IKONOS imagery to estimate surface soil property variability in two Alabama physiographies: Soil Science Society of America Journal, 69, 1789-1798.

Tang, Q., Vivoni, E.R., Muñoz-Arriola, F., Lettenmaier, D.P., 2012, Predictability of evapotranspiration patterns using remotely-sensed vegetation dynamics during the North American monsoon: Journal of Hydrometeorology, 13, 103-121.

Tromp-van Meerveld, H.J., McDonnell, J.J., 2006, On the interrelations between topography, soil depth, soil moisture, transpiration rates and species distribution at the hillslope scale: Advances in Water Resources, 29(2), 293-310.

Van Genuchten, M.T., 1980, Predicting the hydraulic conductivity of unsaturated soi: Soil Science Society of America, 892-898

Vivoni, E.R., Ivanov, V.Y., Bras, R.L., Entekhabi, D., 2004, Generation of triangulated irregular networks based on hydrological similarity: Journal of Hydrologic Engineering, 9(4), 288-302.

Vivoni, E.R., Gutiérrez-Jurado, H.A., Aragón, C.A., Méndez-Barroso, L.A., Rinehart, A.J., Wyckoff, R.L., Rodríguez, J.C., Watts, C.J., Bolten, J.D., Lakshmi, V., Jackson, T.J., 2007a, Variation of hydrometeorological conditions along a topographic transect in northwestern Mexico during the North American monsoon: Journal of Climate, 20(9), 1792-1809.

Vivoni, E.R., Entekhabi, D., Bras, R.L., Ivanov, V.Y., 2007b, Controls on runoff generation and scale-dependence in a distributed hydrologic model: Hydrology and Earth System Sciences, 11, 1683-1701.

Vivoni, E.R., Di Benedetto, F., Grimaldi, S., Eltahir, E.A.B., 2008a, Hypsometric control on surface and subsurface runoff: Water Resources Research, 44, W12502, DOI:10.1029/2008WR006931.

Vivoni, E.R., Gebremichael, M., Watts, C.J., Bindlish, R., Jackson, T.J., 2008b, Comparison of ground-based and remotely-sensed surface soil moisture estimates over complex terrain during SMEX04: Remote Sensing of Environment, 112(2), 314-325.

Vivoni, E.R., Rodríguez, J.C., Watts, C.J., 2010, On the spatiotemporal variability of soil moisture and evapotranspiration in a mountainous basin within the North American monsoon region: Water Resources Research, 46, W02509, DOI:10.1029/2009WR008240.

Vivoni, E.R., Mascaro, G., Mniszewski, S., Fasel, P., Springer, E.P., Ivanov, V.Y., Bras, R.L., 2011, Real-world hydrologic assessment of a fully-distributed hydrological model in a parallel computing environment: Journal of Hydrology, 409, 483-496.

Vivoni, E.R., 2012, Diagnosing seasonal vegetation impacts on evapotranspiration and its partitioning at the catchment scale during SMEX04-NAME: Journal of Hydrometeorology, 13, 1631-1638.

Weiler, M., McDonnell, J.J., 2006, Testing nutrient flushing hypotheses at the hillslope scale: A virtual experiment approach: Journal of Hydrology, 319(1-4), 339-356.

Xiang, T., Vivoni, E.R., Gochis, D.J., 2014, Seasonal evolution of ecohydrological controls on land surface temperature over complex terrain: Water Resources Research, 50, 3852-3874.

Zhang, R., Warrick A.W., Myers, D.E., 1992, Improvement of the prediction of soil particle size fractions using spectral properties: Geoderma, 52, 223-234.

Manuscript received: May 21, 2015
Corrected manuscript received: August 31, 2016
Manuscript accepted: September 13, 2016